Spatiotemporal Distributions of Icebergs in a Temperate Fjord: Columbia Fjord, Alaska

Sarah U. Neuhaus[1], Slawek M. Tulaczyk[1], Carolyn Branecky Begeman[1,2]

[1]Earth and Planetary Sciences, University of California Santa Cruz, Santa Cruz, CA, 95060, USA
5 [2]Los Alamos National Laboratory, Los Alamos, NM, 87545, USA

Correspondence to: Sarah U. Neuhaus (suneuhau@ucsc.edu)

Abstract. Much of the world's ice enters the ocean via outet glaciers terminating in fjords. Inside fjords, icebergs may affect glacier-ocean interactions by cooling incoming ocean waters, enhancing vertical mixing, or by providing back stress
10 on the terminus. However, relatively few studies have been performed on iceberg dynamics inside fjords, particularly outside of Greenland. We examine icebergs calved from Columbia Glacier, Alaska, over eight months spanning late winter to mid-fall using 0.5-meter resolution satellite imagery, identifying icebergs based on pixel brightness. Iceberg sizes fit a power-law distribution with an overall power-law exponent, m, of -1.26 ± 0.05. We find that iceberg calving rate, rather than water temperature, appears to be the major control on the exponent value. We also examine iceberg spatial distribution
15 inside the fjord, and find that large icebergs ($10,000 \text{ m}^2 - 100,000 \text{ m}^2$ cross-sectional area) have low spatial correlation with icebergs of smaller sizes due to their tendency to ground on the shallows. We estimate the surface area of icebergs in contact with incoming seawater to be $2.8 \pm 0.58 \times 10^4 \text{ m}^2$. When compared with our estimated terminus surface area, $9.7 \pm 3.7 \times 10^5$ m^2, we expect iceberg impact on the heat content of the incoming seawater to be negligible in this fjord. Results from our study indicate that if icebergs represent an important factor in controlling glacier-ocean interactions in Greenland fjords,
20 future climate and ocean warming towards conditions similar to those in Coloumbia Fjord will also diminish the role of icebergs in modulating such interactions.

1 Introduction

In recent decades, fjord-terminating glaciers have been rapidly losing mass (Larsen et al., 2007; Pritchard et al., 2009), contributing significantly to eustatic sea level rise (Gardner et al., 2013; McNabb and Hock, 2014). High volumes of
25 ice discharge due to iceberg calving and submarine melt have been attributed to contact with relatively warm and salty fjord waters (Bartholomaus et al., 2013; Motyka et al., 2003). Current fjord circulation models do not take icebergs into account, though icebergs may modify warm, dense waters entering the fjord by enhancing vertical mixing and heat extraction accompanying iceberg melt (Carroll et al., 2015; Klinck et al., 1981; Mortensen et al., 2018; Motyka et al., 2003; Rignot et al., 2010). Various studies have examined the iceberg calving process (Bahr, 1995; Chapuis and Tetzlaff, 2014; Hughes,
30 2002; O'Neel et al., 2003; Warren et al., 2001), as well as the transport and evolution of icebergs in the open ocean (Bigg et

al., 1997; Dowdeswell and Forsberg, 1992; Gladstone et al., 2001; Kubat et al., 2007), but comparably little is known about iceberg transformation occurring inside the fjords where they originate.

Recent studies of icebergs have focused on icebergs calved from Greenland or Antarctic glaciers, however in this study we provide insight into the size and location of icebergs in a major Alaskan fjord using high-resolution satellite

5   imagery. We examine the differences in iceberg populations over a span of eight months in 2013 to gain insights into the seasonal influence on iceberg size distribution. We also investigate how icebergs of varying sizes evolve along the fjord to better understand where iceberg meltwater is introduced in vertical and horizontal dimensions.

Our analyses focus on the fjord of Columbia Glacier, which connects with Prince William Sound (PWS), Alaska. Columbia Glacier is the single largest contributor to ice loss from Alaskan glaciers, accounting for ~6-17% of annual land

10   ice loss from this region (Gardner et al., 2013; Pfeffer, 2015; Rasmussen et al., 2011). Columbia Glacier is also one of the best-studied glaciers in the world. The United States Geologic Survey (USGS) has been instrumenting Columbia Glacier since the 1970's, and the first time-lapse cameras used to study glacier movement and iceberg calving were implemented in 1978 (Meier and Post, 1978; Pfeffer, 2012). From 2012 to 2015, the Prince William Sound Regional Citizen's Advisory Council (PWSRCAC) commissioned a study of Columbia Glacier, which included several field campaigns and geophysical

15   tools, with the aim of better predicting the future behavior of the glacier. PWSRCAC was particularly interested in understanding iceberg discharge, as icebergs that exit Columbia Fjord later intrude on the shipping lanes into and out of the Port of Valdez (Pfeffer, 2012, 2013a, 2013b, 2014a, 2014b, 2015). Because water temperatures at present tend to be warmer in PWS (ranging from ~3 to ~14 ºC) than the ocean waters around Greenland (ranging from ~0 to ~5ºC) (Campbell, 2018; Holland et al., 2008), Columbia Fjord represents a potential analog for Greenland fjords under future warmer climates. We

20   compare our findings to those of recent similar studies of Greenland fjords in order to glimpse what changes might occur in the future in Greenlandic fjords.

Columbia Glacier has a total surface area around 910 km^2 (McNabb et al., 2012a), and is located in central Alaska in the Chugach Mountains (Fig. 1). From 1794 – when the terminus of Columbia Glacier was first mapped by Captain George Vancouver – to 1980, the terminus of the glacier was in a stable location, terminating at the northern end of Heather

25   Island (Meier and Post, 1978; Post, 1975). From 1980 to 2013, the year when the satellite images used in this project were acquired, the glacier retreated approximately 20 km. This retreat revealed a fjord extending north-south, roughly 5 km in width and 20 km in length. At the entrance to the fjord is a submarine end moraine – which shall be referred to as "Heather Moraine" – built by the glacier when it was in its extended Neoglacial position (Meier and Post, 1978). An oceanographic survey of Columbia Fjord completed in 1983 determined that the water column over Heather Moraine was shallow – less

30   than 20 m below Mean Lower Low Water (MLLW) and partially exposed (Pfeffer, 2013a; Walters et al., 1988). Pfeffer (2013a) examined more recent bathymetric surveys of Heather Moraine and found that the bathymetry did not change significantly between 1977 and 2005, indicating that very little erosion has occurred. The mean tidal fluctuation in nearby Valdez, as measured by the National Oceanographic and Atmospheric Administration (NOAA), is ~3m, with maximum fluctuations up to 5-6m, indicating the maximum water depth above Heather Moraine to be ~25m. Behind Heather Moraine,

35   fjord bathymetry descends to 200 m b.s.l. (Walters et al., 1988). After the initial increase in iceberg calving following the

initiation of glacial retreat reached a maximum of over 10 km^3 yr^{-1} in 1999-2000 (Pfeffer, 2013b) – 8.5 km^3 yr^{-1} averaged over 1996-2007 (Rasmussen et al., 2011) – calving rates at Columbia Glacier have been decreasing (Pfeffer, 2013b). Between 2010 and 2013 the average ice flux into the fjord was measured at 2.23 km^3 yr^{-1} (Pfeffer, 2013b), most of which came from the main branch of the glacier. Between 2011 and 2014 the average mass flux from the main branch of Columbia

5 Glacier was measured to be 1.18 ± 0.30 Gt yr^{-1} (~1.29 km^3 yr^{-1}) (Vijay and Braun, 2017).

2 Methods

2.1 Image Processing

In order to determine the spatial distribution of icebergs, we obtained 0.5 m-resolution, 8-bit, grayscale imagery of Columbia Fjord from the Polar Geospatial Center at the University of Minnesota. The images were taken by the WorldView

10 satellites 1 and 2 during 2013, and georeferenced by the Polar Geospatial Center (image details shown in Table 1). Although the WorldView 2 satellite offered multispectral bands, we only used the higher-resolution panchromatic bands from both satellites (WorldView 1 spectrum spanned wavelengths 400 – 900 nm, and WorldView 2 spectrum spanned wavelengths 450 – 800 nm). The spread of dates provides seasonal coverage of the fjord, from late winter (March 13) to the middle of the fall (November 19). Although the majority of the satellite images captured only part of the fjord, we mosaiced overlapping

15 images taken simultaneously or within hundredths of a second to provide complete coverage of the fjord in all but two cases. Given that timescales of iceberg motion are much longer than hundredths of a second, we believe we are justified in using images taken hundredths of a second apart in the same mosaic. The data consists of ten image mosaics spanning six dates, covering much of the seasonal cycle in this area: March 13, May 6, June 10, July 11, July 12, and November 19. We consider the fjord to be the area bounded by the shores of the fjord, the glacier termini, and Heather Moraine (covering a

20 total area of ~87 km^2 [8.7 x10^7 m^2]). Because of the shallow water depths above Heather Moraine, it is a natural barrier separating Columbia Fjord from PWS. In addition, the shallow depths cause large icebergs to run aground, allowing for easy identification of the submarine moraine in the satellite imagery.

To identify and locate icebergs in each image we created a thresholding algorithm using the MATLAB image processing toolbox that identified potential iceberg areas based on pixel intensity value. Icebergs had higher pixel brightness

25 values than the darker fjord waters, thus we set a threshold brightness value above which pixels were classified as icebergs and below which they were classified as water. Because frequency histograms of pixel brightness did not reveal a bimodal pattern, we therefore chose a threshold value of 41 out of 255, which corresponded with the highest pixel value for open ocean identified through visual inspection. The automatic iceberg recognition algorithm performance was impacted when the icebergs were surrounded by ice mélange, a slushy mixture of snow and ice floating on top of the water. Since the

30 mélange was brighter than the water, but darker than the icebergs, we were able to mitigate this by adjusting the threshold value in those areas until we reached a more realistic discrimination of icebergs based on visual inspection. We manually inspected the automatically-selected icebergs to quantify the reliability of automatic iceberg detection. We treat visual inspection as the 'gold standard' because the human observer can use textural and contextual information in addition to

brightness alone. However, we opt for an automatic detection of icebergs for this study because mapping of all icebergs by visual inspection would be prohibitively time consuming.

In addition to defining the pixel intensity threshold, we set upper and lower bounds on the iceberg area, with the lower bound corresponding to the smallest group of pixels we could visually identify as an iceberg (20 pixels, or 5 m^2) and

5   the upper bound corresponding to the number of pixels in the largest iceberg we found visually (112,000 pixels). We set an upper bound on iceberg size to prevent large areas of ice mélange being identified as a single iceberg. The term 'iceberg' in this study refers to icebergs (>15m across as defined by the Canadian Ice Service, or >3000 ft^2 [278 m^2] in area as defined by the US National Ice Service), as well as growlers and bergy bits (glacially-derived ice in the ocean that is smaller than an iceberg). Given the lack of sea ice observed in our satellite imagery, in this study the term 'mélange' refers to tiny chunks of

10   ice derived icebergs or the glacier terminus.

To quantify the error on iceberg identification, we compared the results of the manual and automatic iceberg identification. We divided each mosaic into a test grid, with each test cell being 250 by 250 pixels (~125m x 125m, or roughly half the area of the largest iceberg). We then randomly selected test cells on each of the mosaics and counted the number of icebergs by eye and using the thresholding code. After examining a total of 107 grid cells, we found that the

15   algorithm identified 95 ± 4 % of the icebergs identified by an observer. Occasionally, when icebergs were close together, the algorithm would categorize them as a single iceberg, leading to the under-identification of the number of icebergs. To verify if we had counted enough cells, we divided the cumulative number of icebergs identified by the algorithm in cells 1 through N (where N is the number of test cells counted) by the cumulative number of icebergs identified manually (cells 1 through N), and plotted this versus N (Fig. 2). The slope of the line plateaued around N=44. We used the mean and the standard

20   deviation of the line between N=44 and N=107 as our estimate of iceberg identification error. Error in automatic iceberg identification was greater in mélange-covered areas than open ocean. We found that the algorithm identified 67 ± 6 % of the icebergs in the areas of ice mélange.

In addition to quantifying the error in the number of icebergs identified, we estimated the error on the area of the icebergs by comparing the total area of icebergs calculated by the algorithm. For June 10a and June 10b, the difference in

25   total iceberg area amounted to less than 8% of the total calculated iceberg area for each image. For July 12a and July 12b, that difference amounted to less than 4%. The difference in the total iceberg area was much larger for November 19a and November 19b, which is due to the algorithm identifying areas of open water as ice in the November 19a image. We adjusted the threshold between ice and water for this image, but were not able to completely alleviate the problem.

2.2 Overall Iceberg Distributions

30   To examine the spatial distribution of icebergs inside the fjord, we created a time-integrated map of iceberg density. We did this by dividing the fjord into 500 m x 500 m squares and counting the number of icebergs whose centroids were present within each square. Overlaying the results from March 13, June 10a, July 12a, and November 19a, we created a map which depicted the locations of all the icebergs identified during our study. We created a similar map of cumulative area of icebergs whose centroids resided in each square.

2.3 Along Fjord Iceberg Distributions

To examine the variation in spatial distribution of icebergs between scenes, we divided the fjord longitudinally into evenly spaced sections roughly one kilometer in length starting from the terminus to Heather Moraine. The icebergs were binned into those sections based on the location of their centroids. In some of our analyses, we needed a larger sample size of icebergs, so we also divided the fjord into three geographic sections (Fig. 1). The "Proximal Zone" spans from the terminus of the glacier to the first major constriction, the "Mid-Fjord Zone" spans from the constriction to the inlet on the east side of the fjord, roughly two-thirds of the way downfjord, and the "Distal Zone" spans from the inlet to Heather Moraine.

Following what other studies have done, we fit a power-law equation of the form $Pr(A > a) = bA^m$ to iceberg areas in each of the three zones to determine the iceberg size-distribution (Kirkham et al., 2017; Sulak et al., 2017; Tournadre et al., 2016). $Pr(A > a)$ represents the number of icebergs whose area, A, is greater than a. b and m are the constants which are constrained by data fitting. We chose values of a from 0 to 100,000 m², subdividing the bin from 0 to 1000 m² into 10, 25, 50, 75, 100, 250, 500, and 750 m². To determine the goodness of fit of the power-law we performed a Kolmogorov-Smirnov test. In order to obtain a fit with 95% confidence we had to remove the largest icebergs, which deviate from the power-law size distribution followed by smaller icebergs. This has also been done in other similar recent studies (e.g. Sulak et al., 2017). An example of our power-law fit is shown in Fig. 3.

To test whether icebergs of various sizes co-vary spatially within Columbia Fjord, we separated the iceberg population into five class sizes based on their waterline cross-sectional area. The class size bins were spaced logarithmically (0-10 m², 10-100 m², 100-1,000 m², 1,000-10,000 m², and 10,000-100,000 m²) with Class 1 representing the smallest icebergs and Class 5 representing the largest. For each one-kilometer bin along the fjord we compared the evolution of the different classes down the fjord by plotting the different class sizes against each other and calculating the Pearson correlation coefficient using the equation:

$$P_{C_a C_b} = \frac{cov(C_a, C_b)}{\sigma_{C_a} \sigma_{C_b}} \qquad \qquad \text{Eq. (1)}$$

where cov is the covariance, σ is the standard deviation, and C_a and C_b represent the two class sizes being compared. The limits of the 95% confidence interval were used as the upper and lower bounds of the error. We calculated the Pearson correlation coefficient using the icebergs from all scenes combined. In addition to calculating the correlation of the different size classes, we plotted the exact locations of the large icebergs (Classes 3-5) inside the fjord for each date to better understand where the large icebergs were located inside the fjord.

2.4 Iceberg Characteristics

We use the area of the icebergs visible from the satellite imagery (A), which we refer to as the waterline cross-sectional area, as a proxy for iceberg volume. However, we also estimate iceberg volume using two previously proposed scaling laws. For the first approach we use the equation for iceberg volume (V) derived by Sulak et al. (2017):

$$V = 6.0A^{1.30} \qquad \qquad \text{Eq. (2)}$$

For the second approach we assume the icebergs to be rectangular prisms and use the proportions used by Bigg et al. (1997) where the ratio of iceberg length to width is equal to 1.5:1, the draught to the width ratio equal to 1:1, and the draught to freeboard ratio equal to 5:1. The equation relating area to volume using these dimensions is:

$$V = 0.98A^{1.5} \qquad \text{Eq. (3)}$$

We also use the dimensions outlined in Bigg et al. (1997) to estimate keel depth (k) of the icebergs with the equation:

$$k = 0.67A^{0.5} \qquad \text{Eq. (4)}$$

We calculated the relative increase in the fjord albedo due to the presence of ice for each scene by assigning an albedo of 0.60 for each pixel identified as ice (Zeng et al., 1984) and 0.060 for the remaining pixels representing ocean surface. In this way, icebergs as well as mélange were taken into account. The selected albedo of fjord water is the monthly averaged albedo for ocean water surface for the months of April, May, June, August, and September for the latitude of Columbia Fjord (Payne, 1972).

3 Results

3.1 Overall Iceberg Distributions

During 2013, the majority of icebergs were found within the first 5 km of the terminus, corresponding to the area of the fjord prior to where the fjord coastline pinches in and forms a constriction (Fig. 4a). Beyond the constriction, the number of icebergs drop steeply (Fig. 4a). Iceberg area followed a similar pattern, with the majority of iceberg area in the first 5 km from the terminus, followed by a rapid decline in total iceberg area on the other side of the constriction (Fig. 4b and Fig. 5). All scenes show a peak in the total iceberg area not directly adjacent to the terminus, but 2 to 5 kilometers away. Most icebergs were small; over 95% of all the icebergs counted here had a waterline cross-sectional area of 100 m^2 or less (Fig. 5). One source of uncertainty in our results is the misidentification of mélange as large icebergs. In order to assess the amount of mélange present in Columbia Fjord, we examined the pixels identified as ice, but not counted as icebergs. The mélange coverage in the spring and fall months was similar ($3.2 \pm 1.9 \times 10^6$ m^2), whereas the mélange coverage in the summer months was $9.1 \pm 0.8 \times 10^6$ m^2.

3.2 Along Fjord Iceberg Distributions

The exponents from the power-law equations fit to the iceberg size distributions varied both seasonally and spatially, indicating a pattern in both the spatial and seasonal size distributions of icebergs inside the fjord. The power exponent represents the relative abundance of large versus small icebergs, with more negative power exponent values indicating a higher proportion of small icebergs. The power exponents for the spring and fall months were similar, whereas the power exponents were more negative for the summer scenes. The power exponent for the spring and fall months ranged from -1.24 ± 0.03 to -0.91 ± 0.02 with a mean of -1.10. In the summer scenes, the power exponent ranged from -1.54 ± 0.03 to -1.12 ± 0.07 with a mean of -1.35. Every scene showed a decrease in the power-law exponent from the Proximal Zone to the Mid-Fjord Zone – indicating a decrease in the proportion of large icebergs with distance from the glacier terminus – and

a subsequent increase in the power-law exponent from the Mid-Fjord Zone to the Distal Zone indicating an increase in the proportion of large icebergs near Heather Moraine (Fig. 6). The average decrease in the power exponent from the Proximal-Fjord to the Mid-Fjord Zone was 0.16, and the average increase from the Mid-Fjord Zone to the Distal Zone was 0.24.

We calculated the spatial correlation of the different iceberg size classes along the fjord to reveal similarities and differences in iceberg evolution down the fjord. The correlation coefficient reflects the spatial covariance of different iceberg size classes. We performed these calculations for each scene individually, and for all identified icebergs combined. Our results show that the largest iceberg class, with a waterline cross-sectional area between 10,000 and 100,000 m^2, is the least spatially correlated with the other classes (correlation coefficient ranging between $0.345^{+0.125}_{-0.138}$ and $0.490^{+0.105}_{-0.122}$; Table 2). In contrast, the other class sizes are highly spatially correlated with each other (correlation coefficients ranging between $0.809^{+0.046}_{-0.058}$ and $0.989^{+0.005}_{-0.007}$; Table 2). After calculating the spatial correlation of the iceberg classes for each scene independently, we determined that the correlation does not appear to be seasonally variable.

3.3 Iceberg Volume and Effects on the Fjord

The two methods we used to calculate iceberg volume yielded slightly different results (see Table 3). Generally, the volume calculations using Eq. (3) were larger than the volume calculations using Eq. (2). Both methods found that the icebergs with waterline surface areas greater than 1000 m^2 accounted for the majority of the total ice volume present in each scene. Using Eq. (3), the percentage of ice volume that the large icebergs contained ranged from 53% to 89%, and using Eq. (2), the percentage of ice volume that the large icebergs contained ranged from 35% to 70%.

The estimated increase in albedo due to the presence of icebergs for Columbia Fjord ranged from 1.2% to 9.8% (Table 4). The albedo increase was highest in the summer months, corresponding to the increased presence of ice inside the fjord.

In order to further assess the potential for icebergs to affect the fjord waters, we estimated the iceberg residence time inside the fjord, neglecting iceberg melt. We did this by comparing the average annual calving rate for both arms of Columbia Glacier (Pfeffer, 2013b) to the volume of ice inside the fjord. The average residence time was 15 ± 5 days using Eq. (3) to calculate iceberg volume, and 13 ± 6 days when using Eq. (2). These estimates represent the lower bound for the iceberg residence times because we do not account for the volume of ice lost due to melt.

4 Discussion

4.1 Overall Iceberg Distributions

Our data reveal spatial patterns in iceberg distribution in Columbia Fjord in 2013. In general, iceberg coverage decreases with distance from the terminus. The observed spike in iceberg ice coverage 2 to 5 km from the terminus (Fig. 5) is somewhat surprising given that icebergs originate at the terminus, and it would be logical to expect the highest concentration of icebergs to be immediately adjacent to the terminus. Potential explanations for this are that the kinetic energy associated with the calving process or the inflow of subglacial meltwater at the grounding line pushes icebergs away

from the terminus. Further evidence for this is the fact that when we normalized the total iceberg area to bin area, only the summer months (which have higher subglacial meltwater discharge) showed peak iceberg concentration away from the terminus. Alternatively, these patterns of ice concentration in the fjord could be the result of influx of icebergs from the west arm of Columbia Glacier. Figures 4a and 4b show an increase in both the number and area of icebergs in the location where

5 the west arm of Columbia Glacier contacts the fjord. Additionally, circulation patterns within the fjord could be driving these patterns of ice congregation. Near the terminus the fjord is wide, but roughly 4 to 6 km downfjord it narrows to ~2 km before expanding out to a consistent width of ~4.5 km until Heather Moraine. This change in geometry may drive circulation patterns that concentrate icebergs 2-5 km from the terminus.

In addition to these spatial patterns there were seasonal differences in iceberg coverage in Columbia Fjord in 2013,

10 with more icebergs present during the summer months than the spring or fall (Fig. 5). This is consistent with an increase in calving rates caused by warmer air and water temperatures. Warmer fjord waters may increase the rate of submarine melt, which then increases the iceberg calving rates (Luckman et al., 2015; O'Leary and Christoffersen, 2013). In addition, surface meltwater caused by warmer air temperatures can aid the formation of icebergs by infiltrating and enlarging crevasses at the terminus (Van Der Veen, 1998; Weertman, 1973). These processes may all work together to produce

15 increased ice discharge during warm summer months as opposed to the late winter and fall. In calculating the calving rate of Columbia Glacier in 2013, Vijay and Braun (2017) show an increase in the calving rate from March until June/July, followed by a decrease in the calving rate for the remainder of the year. This increased ice discharge would explain increased iceberg coverage during the summer.

4.2 Along Fjord Iceberg Distributions

20 We fit power-law distributions to the data to gain insight – both seasonally and spatially – into the size-distributions of icebergs inside the fjord. Fitting a power-law distribution to the data allows us to more quantitatively understand the spatiotemporal differences in iceberg size distribution because power-law exponents reflect the relative abundance of small icebergs versus large icebergs. Our iceberg distributions were better described by a power-law distribution than lognormal, which is consistent with the conclusion from Kirkham et al. (2017) that icebergs near the calving front tend toward a power-

25 law distribution, and icebergs further out in the open ocean fit a lognormal distribution. Power-law exponents indicate a decrease in the relative proportion of large icebergs in the Mid-Fjord Zone compared to the Proximal Zone. This is unsurprising given that we would expect icebergs to melt or fracture rather than grow as they travel from the terminus (Fig. 6). We interpret the increase in the proportion of large icebergs in the Distal Zone to be due to the influence of Heather Moraine which grounds large icebergs because it is at most 25 m below the sea surface (Pfeffer, 2013a; Walters et al., 1988).

30 The larger icebergs become grounded until they have melted or broken up sufficiently to pass over, or they are pushed over by strong winds or allowed passage during high tides (Pfeffer, 2015).

Power-law exponents also indicate that there is a greater proportion of smaller icebergs present throughout the fjord in the summer months, including within the Proximal Zone near the terminus. This could indicate that the glacier calves smaller icebergs in the summer. During the summer when air temperatures are higher, meltwater is ubiquitous along the

surface of the glacier and can help break calving ice into smaller pieces through hydrofracturing (Van Der Veen, 1998). Alternatively, the icebergs could be more prone to melt and fragmentation during the summer, which would lead to the increase of small icebergs in the Proximal Zone. Smaller cracks present in icebergs that formed prior to calving could assist the break-up of icebergs by opening up in response to the changes in stresses acting on the ice once it enters the water. In

5 addition, warmer fjord waters present in the summer could increase the overall iceberg melt, reducing iceberg size in the summer.

We compared the power-law exponents from Columbia Glacier to those calculated for other glaciers in order to determine the factors that influence iceberg size distribution. Sulak et al. (2017) reported a power-law exponent of -2.00 ±0.06 for Sermilik Fjord, a power-law exponent of -1.87 ±0.05 for Rink Isbrae Fjord, and a power-law exponent of -1.62 ±

10 0.04 for Kangerlussuup Sermia Fjord. Kirkham et al. (2017) reported a power-law exponent of -2.4 for the icebergs near the calving front of Jakobshavn Isbrae, Ilulissat Icefjord. These studies found their power exponents using the icebergs in the entire fjord, therefore we also calculated the power exponent for all of Columbia Fjord, and averaged our results to produce a value of -1.26 ± 0.05 for the entire study. We found no discernible relationship between power-law exponents and seawater temperatures, however, there is a relationship between power-law exponents and average annual calving flux (Howat et al.,

15 2011; Sulak et al., 2017; Vijay and Braun, 2017). A higher calving flux corresponded to a more negative power-law exponent; glaciers with higher discharge rates had higher proportions of small icebergs (Fig. 7). This supports the suggestion of Sulak et al. (2017) that the power-law exponent could be an indicator of glacier productivity, i.e. calving rate.

In calculating the spatial correlation of icebergs inside the fjord, we found that the majority of icebergs followed similar spatial patterns, but that the largest iceberg class was not strongly spatially correlated to any of the other size classes.

20 The largest icebergs contain the majority of the ice inside the fjord, yet they behave differently than the smaller icebergs. Our interpretation of this lack of correlation is that the largest icebergs are running aground on the shallower areas of the fjord, which decouples their spatiotemporal evolution from the smaller icebergs that tend to float more freely. Bathymetric surveys (McNabb et al., 2012a) show that in addition to being shallow along the sides and at Heather Moraine, the fjord contains areas near the terminus with depths around 75 m which are able to ground icebergs with waterline cross-sectional

25 areas larger than roughly 8,500 m^2 [Eq. (4)]. We found that the largest icebergs were located in those shallower areas (Fig. 8). The fact that the largest icebergs behave differently along the fjord than the other icebergs further justifies removing the largest icebergs from the dataset when fitting the power-law equation for size-frequency distribution.

4.3 Iceberg Effects on the Fjord

Most iceberg volume is found in relatively few icebergs. Icebergs with a waterline cross-sectional area greater than

30 1000 m^2 (Classes 4 and 5) accounted for less than one percent of the number of icebergs present in the fjord, yet they made up 53-89% of the total iceberg volume in the fjord [Eq. (3)]. This has implications for where freshwater is added to the fjord. Intuition suggests that freshwater would mainly be introduced to the fjord near the terminus where most of the icebergs reside and the front of the glacier is in contact with the ocean water. While a majority of the iceberg area can be

found within the first five kilometers of the fjord Fig. 4b, the largest icebergs also tend to be located in the shallow areas of the fjord (Fig. 8). As a result, freshwater is being introduced in those areas as well.

Icebergs may have the ability to affect the dynamics of the fjord in which they reside by interacting with the deeper fjord waters that have not yet reached the terminus. Because the latent heat of fusion for ice (~335,000 J kg^{-1}) is much

5 greater than the specific heat capacity of water (~4,180 J kg^{-1} K^{-1}), melting a small amount of ice decreases the temperature of a much larger volume of liquid water. Water circulation inside fjords is often represented with a simple 2-D model of buoyancy-driven circulation, in which warm, dense salt water flows into the fjord until it reaches the terminus. There it melts ice and mixes with the resulting fresh water, producing a buoyant layer of colder and less salty water that flows seaward along the fjord surface (Motyka et al., 2003). Salinity profiles taken in the middle of the fjord indicate that the

10 transition from the fresher surface layer to the saltier incoming water is at about 10 m depth (Arimitsu et al., 2017). A small fraction (2.4% by number) of all the icebergs we found in our study are large enough that their keels reach the incoming water layer, based on our calculations of keel depths [Eq. (4)]. If these icebergs persist long enough without breaking up, they have the potential to cool the incoming water before it reaches the terminus, thus affecting the rate of submarine melting at the terminus. In addition, large icebergs (area of $\geq$ 600 m^2) get hung up on Heather Moraine. The warm water entering

15 Columbia Fjord is forced to spill over Heather Moraine, therefore increasing interactions with the surfaces of grounded icebergs, potentially resulting in a reduction in the temperature and salinity of the inflowing water.

We also expect icebergs to have a cooling effect on the upper, outgoing water layer. The majority of ice volume resides in this layer, and icebergs can extract heat from this layer as they melt. In addition, the presence of icebergs lowers the amount of solar radiation absorbed by the fjord by increasing the albedo (from a 1.2 % increase in November to 9.8% in

20 June). The upper layer experiences the most solar heating and is thus affected the most by the increased albedo from the icebergs.

4.4 Comparison to Greenland Fjords

Columbia Fjord differs from fjords studied in Greenland that have glaciers with comparable terminus velocities. The Greenland Ice Sheet contains roughly 2.85 x 10^6 km^3 of ice (IPCC, 2001), and much of that ice drains out to the open

25 ocean through fjords. Because of this vast amount of ice, many studies of icebergs in fjords have focused their attention on Greenland (Enderlin et al., 2016; Enderlin and Hamilton, 2014; Kirkham et al., 2017; Moon et al., 2018; Sulak et al., 2017).

A large difference between our study site and the sites in Greenland is the presence of sea ice. Winter sea ice formation helps create a thick mélange by preventing icebergs and bergy bits from exiting the fjord. This mélange not only increases iceberg residence time in the fjord, but also provides a back stress on the terminus that slows the rate of iceberg

30 calving and terminus velocity (Amundson et al., 2010; Walter et al., 2012). In Greenland, winter sea ice formation is widely prevalent (Amundson et al., 2010; Higgins, 1991; Walter et al., 2012), however, sea ice was not present in any of the scenes we examined in detail. Some pancake ice was visible in a satellite image taken on March 26 which was not used in this study, however it was not thick enough to lock in icebergs. This is in spite of the fact that the maximum sea ice extent in the Arctic regions occurs in March. We found that the mélange coverage was greatest in the summer months when the iceberg

coverage was also greatest, however the mélange coverage only amounted to 11%. Hence, ice mélange in Columbia Fjord appears to be more a function of higher summer calving rates than winter-time capture of ice fragments in sea ice. This lack of mélange in Columbia Fjord agrees with our finding that icebergs in Greenlandic fjords appear to have longer residence times. We approximated the iceberg residence times in Columbia Fjord to be roughly a fortnight, but in Greenland icebergs

5   can remain inside fjords for over 100 days (Sulak et al., 2017; Sutherland et al., 2014). The residence times in Greenlandic fjords allow longer interactions between icebergs and the incoming seawater before it reaches the terminus.

In addition, icebergs in Greenlandic fjords tend to be larger. Not only do the larger icebergs remain in existence longer because their smaller surface area to volume ratio reduces melting, their deeper keels allow for more contact with – and thus more cooling of – the incoming warmer ocean waters. The largest icebergs in our study have a waterline cross

10   sectional area on the order of magnitude 10^4 m^2, whereas other studies have measured icebergs to be around 10^7 m^2 (Kirkham et al., 2017; Sulak et al., 2017). A primary reason for the smaller icebergs in Columbia Fjord is the height of the calving front. Vijay and Braun (2017) measured the maximum thickness of the terminus to be 305 m between July 2011 and July 2014. One consequence of the smaller icebergs is the reduced presence of icebergs that penetrate the lower, incoming water layer. Using the iceberg geometry from Eq. (3) we estimate the iceberg surface area in contact with the incoming waters,

15   averaged over all the dates, to be 2.8 ± 0.58 x 10^4 m^2. This is contrasted with the surface area of the terminus (9.7 ± 3.7 x 10^5 m^2) which we calculated by taking profiles of ice thickness near termini of the main and west arms of Columbia Glacier using the ice thickness data published in McNabb et al. (2012b). This is a conservative estimate of terminus area because we do not account for the sinuosity or roughness of the terminus. We also do not account for the roughness of the icebergs in our calculations of iceberg surface area, but we do not expect them to be significantly rougher than the calving front.

20   Because we estimate the surface area of the terminus to be approximately two orders of magnitude greater than the surface area of icebergs in contact with the incoming water, with the exception of the icebergs stranded on Heather Moraine, the icebergs are not contributing as much to the cooling of the ocean waters as the terminus itself. However, studies in Greenland have found the opposite – the surface area of icebergs is much greater than the surface area of the terminus and therefore must play a larger role in fjord circulation dynamics (Sulak et al., 2017).

25   The combination of the presence of sea ice, larger icebergs, and higher residence times means that the icebergs in Greenlandic fjords have a greater potential to cool the incoming water before it reaches the terminus. However, if the warming trend that we have seen in the waters making their way to Greenland persists, retreat and thinning at the terminus could cause the fjords in the southern part of Greenland to resemble current Alaskan fjords like Columbia; namely, the warmer waters would prevent the formation of a terminus-buttressing mélange, and the thinner terminus would produce

30   smaller icebergs. This may represent a positive feedback during climate warming as the decreasing size and residence time of large icebergs decreases their ability to cool incoming ocean waters.

5 Conclusion

In this study we have obtained constraints on the distributions of icebergs inside a large Alaskan temperate fjord with high calving fluxes. The majority of icebergs were found within five kilometers of the terminus, but peak iceberg

frequency was reached a few kilometers away from the terminus, particularly in the summer. The iceberg distributions fit a power-law distribution as opposed to a lognormal distribution. The power-law exponents suggest that the icebergs melt or break up as they move away from the terminus, and that large icebergs run aground on Heather Moraine. There is a greater presence of icebergs in the summer months, but those icebergs tend to be smaller. We attribute this to summer hydrological

5 forcing intensifying ice fragmentation through water-filled crevasses. In addition, we find a correlation between power-law exponents and average annual calving rate, with larger calving rates resulting in increased proportions of small icebergs.

Most of the calved ice was contained within only a small fraction of large icebergs. The largest icebergs (which account for the majority of calved ice) are the least spatially correlated with the other iceberg class sizes, which we attribute to their tendency to ground in the shallow areas of the fjord – namely along the sides and on Heather Moraine. The largest

10 icebergs have the greatest potential to cool the incoming ocean waters before they reach the terminus, however, in Columbia Fjord the surface area of the glacier terminus is thought to surpass the surface area of icebergs in contact with the incoming ocean water, rendering the iceberg cooling effect negligible. The total surface area of the icebergs inside the fjord amounts to 2.9% of the terminus surface area. We expect that only the icebergs at Heather Moraine have the potential to affect the dynamics of the fjord since the shallow water column allows more contact between icebergs and the incoming water. The

15 icebergs do have the potential to cool the outgoing upper layer of ocean waters by increasing the albedo in the summer months, and thereby decrease the solar heating.

Alaskan fjords should be studied because their glaciers are currently contributing significantly to sea level rise. In addition, they may serve as a proxy for future Greenlandic fjords under warmer climate scenarios. Current differences between Alaskan and Greenlandic fjords include the lack of sea ice helping to form thick mélange, smaller icebergs, and

20 shorter iceberg residence times. Should the recent warming trend in the ocean waters making their way to Greenland continue (Holland et al., 2008; Straneo and Heimbach, 2013), warmer waters in fjords may prevent the formation of sea ice and thick mélange, which protect the termini from further retreat.

Data Availability

The imagery used in this study are available via the Polar Geospatial Center.

25 **Author Contributions**

SN and ST conceived of the study presented here. SN acquired the data and performed analysis and interpretation of the data with guidance from ST and CB. SN prepared the manuscript with contributions from both ST and CB.

Competing Interests

The authors declare no conflict of interest.

Acknowledgements

This work was partly funded through NASA grant NNX08AD31G. The Polar Geospatial Center provided the satellite imagery used in this study. We would like to acknowledge Shad O'Neel for inspiration and discussion of this study.

5   **References**

Amundson, J. M., Fahnestock, M., Truffer, M., Brown, J., Lüthi, M. P. and Motyka, R. J.: Ice mélange dynamics and implications for terminus stability, Jakobshavn Isbrse, Greenland, J. Geophys. Res. Earth Surf., 115(1), 1–12, doi:10.1029/2009JF001405, 2010.

Arimitsu, M., Piatt, J. and Heflin, B.: Pelagic Forage Fish Distribution Abundance and Body Condition: U.S. Geological

10   Survey data release, , doi:10.5066/F74J0C9Z, 2017.

Bahr, D. B.: Simulating iceberg calving with a percolation model, J. Geophys. Res., 100(B4), 6225–6232, doi:10.1029/94JB03133, 1995.

Bartholomaus, T. C., Larsen, C. F. and O'Neel, S.: Does calving matter? Evidence for significant submarine melt, Earth Planet. Sci. Lett., 380, 21–30, doi:10.1016/j.epsl.2013.08.014, 2013.

15   Bigg, G. R., Wadley, M. R., Stevens, D. P. and Johnson, J. A.: Modelling the dynamics and thermodynamics of icebergs, Cold Reg. Sci. Technol., 26(2), 113–135, doi:10.1016/S0165-232X(97)00012-8, 1997.

Campbell, R. W.: Hydrographic trends in Prince William Sound, Alaska, 1960–2016, Deep. Res. Part II Top. Stud. Oceanogr., 147, 43–57, doi:10.1016/j.dsr2.2017.08.014, 2018.

Carroll, D., Sutherland, D. A., Shroyer, E. L., Nash, J. D., Catania, G. A. and Stearns, L. A.: Modeling Turbulent Subglacial

20   Meltwater Plumes: Implications for Fjord-Scale Buoyancy-Driven Circulation, J. Phys. Oceanogr., 45(8), 2169–2185, doi:10.1175/JPO-D-15-0033.1, 2015.

Chapuis, A. and Tetzlaff, T.: The variability of tidewater-glacier calving: Origin of event-size and interval distributions, J. Glaciol., 60(222), 622–634, doi:10.3189/2014JoG13J215, 2014.

Dowdeswell, J. a. and Forsberg, C. F.: The size and frequency of icebergs and bergy bits derived from tidewater glaciers in

25   Kongsfjorden, northwest Spitsbergen, Polar Res., 11(2), 81–91, doi:10.1111/j.1751-8369.1992.tb00414.x, 1992.

Enderlin, E. M. and Hamilton, G. S.: Estimates of iceberg submarine melting from high-resolution digital elevation models: Application to Sermilik Fjord, East Greenland, J. Glaciol., 60(224), 1111–1116, doi:10.3189/2014JoG14J085, 2014.

Enderlin, E. M., Hamilton, G. S., Straneo, F. and Sutherland, D. A.: Iceberg meltwater fluxes dominate the freshwater budget in Greenland's iceberg-congested glacial fjords, Geophys. Res. Lett., 43(21), 11,287-11,294,

30   doi:10.1002/2016GL070718, 2016.

Gardner, A. S., Moholdt, G., Cogley, J. G., Wouters, B., Arendt, A. a, Wahr, J., Berthier, E., Hock, R., Pfeffer, W. T., Kaser, G., Ligtenberg, S. R. M., Bolch, T., Sharp, M. J., Hagen, J. O., van den Broeke, M. R. and Paul, F.: A reconciled estimate of glacier contributions to sea level rise: 2003 to 2009., Science, 340(6134), 852–7, doi:10.1126/science.1234532, 2013.

Gladstone, R. M., Bigg, G. R. and Nicholls, K. W.: Iceberg trajectory modeling and meltwater injection in the Southern Ocean, J. Geophys. Res., 106(C9), 19903–19915, doi:10.1029/2000JC000347, 2001.

Higgins, A. K.: North Greenland glacier velocities and calf ice production, Polarforschung, 60(1), 1–23, 1991.

Holland, D. M., Thomas, R. H., de Young, B., Ribergaard, M. H. and Lyberth, B.: Acceleration of Jakobshavn
5   Isbræ triggered by warm subsurface ocean waters, Nat. Geosci., 1(10), 659–664, doi:10.1038/ngeo316, 2008.

Howat, I. M., Ahn, Y., Joughin, I., Van Den Broeke, M. R., Lenaerts, J. T. M. and Smith, B.: Mass balance of Greenland's three largest outlet glaciers, 2000-2010, Geophys. Res. Lett., 38(12), 1–5, doi:10.1029/2011GL047565, 2011.

Hughes, T.: Calving bays, Quat. Sci. Rev., 21(1–3), 267–282, doi:10.1016/S0277-3791(01)00092-0, 2002.

Kirkham, J. D., Rosser, N. J., Wainwright, J., Vann Jones, E. C., Dunning, S. A., Lane, V. S., Hawthorn, D. E., Strzelecki,
10 M. C. and Szczuciński, W.: Drift-dependent changes in iceberg size-frequency distributions, Sci. Rep., 7(1), 1–10, doi:10.1038/s41598-017-14863-2, 2017.

Klinck, J. M., O'Brien, J. J. and Svendsen, H.: A Simple Model of Fjord and Coastal Circulation Interaction, J. Phys. Oceanogr., 11(12), 1612–1626, doi:10.1175/1520-0485(1981)011<1612:ASMOFA>2.0.CO;2, 1981.

Kubat, I., Sayed, M., Savage, S. B., Carrieres, T. and Crocker, G. B.: An Operational Iceberg Deterioration Model, Proc.
15 Seventeenth Int. Offshore Polar Eng. Conf., 652–657 [online] Available from: http://nparc.cisti-icist.nrc-cnrc.gc.ca/npsi/ctrl?action=rtdoc&an=12327569, 2007.

Larsen, C. F., Motyka, R. J., Arendt, A. A., Echelmeyer, K. A. and Geissler, P. E.: Glacier changes in southeast Alaska and northwest British Columbia and contribution to sea level rise, J. Geophys. Res. Earth Surf., 112(1), 1–11, doi:10.1029/2006JF000586, 2007.

20 Luckman, A., Benn, D. I., Cottier, F., Bevan, S., Nilsen, F. and Inall, M.: Calving rates at tidewater glaciers vary strongly with ocean temperature, Nat. Commun., 6, 1–7, doi:10.1038/ncomms9566, 2015.

McNabb, R. W. and Hock, R.: Variations in Alaska tidewater glacier frontal ablation, 1985-2013, J. Geophys. Res. Earth Surf., 119(2), 153–167, doi:10.1002/2014JF003276, 2014.

McNabb, R. W., Hock, R., O'Neel, S., Rasmussen, L. a., Ahn, Y., Braun, M., Conway, H., Herreid, S., Joughin, I., Pfeffer,
25 W. T., Smith, B. E. and Truffer, M.: Using surface velocities to calculate ice thickness and bed topography: A case study at Columbia Glacier, Alaska, USA, J. Glaciol., 58(212), 1151–1164, doi:10.3189/2012JoG11J249, 2012a.

McNabb, R. W., Hock, R., O'Neel, S., Rasmussen, L. A., Ahn, Y., Braun, M., Conway, H., Herreid, S., Joughin, I., Pfeffer, W. T., Smith, B. E. and Truffer, M.: Using surface velocities to calculate ice thickness and bed topography: A case study at Columbia Glacier, Alaska, USA, J. Glaciol., 58(212), 1151–1164, doi:10.3189/2012JoG11J249, 2012b.

30 Meier, M. F. and Post, A.: Columbia Glacier Progress Report, , (DECEMBER 1977), 1978.

Moon, T., Sutherland, D. A., Carroll, D., Felikson, D., Kehrl, L. and Straneo, F.: Subsurface iceberg melt key to Greenland fjord freshwater budget, Nat. Geosci., 11(1), 49–54, doi:10.1038/s41561-017-0018-z, 2018.

Mortensen, J., Rysgaard, S., Arendt, K. E., Juul-Pedersen, T., Søgaard, D. H., Bendtsen, J. and Meire, L.: Local coastal water masses control heat levels in a West Greenland tidewater outlet glacier fjord, J. Geophys. Res. Ocean., (123), 1–16,
35 doi:10.1029/2018JC014549, 2018.

Motyka, R. J., Hunter, L., Echelmeyer, K. a. and Connor, C.: Submarine melting at the terminus of a temperate tidewater glacier, LeConte Glacier, Alaska, U.S.A, Ann. Glaciol., 36, 57–65, doi:10.3189/172756403781816374, 2003.

O'Leary, M. and Christoffersen, P.: Calving on tidewater glaciers amplified by submarine frontal melting, Cryosphere, 7(1), 119–128, doi:10.5194/tc-7-119-2013, 2013.

5 O'Neel, S., Echelmeyer, K. A. and Motyka, R. J.: Short-term variations in calving of a tidewater glacier: LeConte Glacier, Alaska, U.S.A, J. Glaciol., 49(167), 587–598, doi:10.3189/172756503781830430, 2003.

Payne, R. E.: Albedo of the Sea Surface, J. Atmos. Sci., 29(5), 959–970, doi:10.1175/1520-0469(1972)029<0959:AOTSS>2.0.CO;2, 1972.

Pfeffer, W. T.: Report to Prince William Sound Citizen's Regional Advisory Council: Future Iceberg Discharge from
10 Columbia Glacier, Alaska - Report 1, , (December), 1–46, 2012.

Pfeffer, W. T.: Report to Prince William Sound Citizen's Regional Advisory Council: Future Iceberg Discharge from Columbia Glacier, Alaska - Report 2, , (June), 1–20, 2013a.

Pfeffer, W. T.: Report to Prince William Sound Citizen's Regional Advisory Council: Future Iceberg Discharge from Columbia Glacier, Alaska - Report 3, , (November), 1–22, 2013b.

15 Pfeffer, W. T.: Report to Prince William Sound Citizen's Regional Advisory Council: Future Iceberg Discharge from Columbia Glacier, Alaska - Report 4, , (October), 1–10, 2014a.

Pfeffer, W. T.: Report to Prince William Sound Citizen's Regional Advisory Council: Future Iceberg Discharge from Columbia Glacier, Alaska - Report 5, , (October), 1–8, 2014b.

Pfeffer, W. T.: Report to Prince William Sound Citizen's Regional Advisory Council: Future Iceberg Discharge from
20 Columbia Glacier, Alaska - Final Report, , (June), 1–20, 2015.

Post, A.: Preliminary hydrography and historic terminal changes of Columbia Glacier, Alaska. [online] Available from: http://pubs.er.usgs.gov/publication/ha559, 1975.

Pritchard, H. D., Arthern, R. J., Vaughan, D. G. and Edwards, L. A.: Extensive dynamic thinning on the margins of the Greenland and Antarctic ice sheets, Nature, 461(7266), 971–975, doi:10.1038/nature08471, 2009.

25 Rasmussen, L. a., Conway, H., Krimmel, R. M. and Hock, R.: Surface mass balance, thinning and iceberg production, Columbia Glacier, Alaska, 1948-2007, J. Glaciol., 57(203), 431–440, doi:10.3189/002214311796905532, 2011.

Rignot, E., Koppes, M. and Velicogna, I.: Rapid submarine melting of the calving faces of West Greenland glaciers, Nat. Geosci., 3(3), 187–191, doi:10.1038/ngeo765, 2010.

Straneo, F. and Heimbach, P.: North Atlantic warming and the retreat of Greenland's outlet glaciers, Nature, 504(7478), 36–
30 43, doi:10.1038/nature12854, 2013.

Sulak, D. J., Sutherland, D. A., Enderlin, E. M., Stearns, L. A. and Hamilton, G. S.: Iceberg properties and distributions in three Greenlandic fjords using satellite imagery, Ann. Glaciol., 58(74), 92–106, doi:10.1017/aog.2017.5, 2017.

Sutherland, D. A., Roth, G. E., Hamilton, G. S., Mernild, S. H., Stearns, L. A. and Straneo, F.: Quantifying flow regimes in a Greenland glacial fjord using iceberg drifters, Geophys. Res. Lett., 41, 8411–8420, doi:10.1002/2014GL062256, 2014.

35 Tournadre, J., Bouhier, N., Girard-Ardhuin, F. and Rémy, F.: Antarctic iceberg distributions 1992-2014, J. Geophys. Res.

Ocean., 121, 327–349, doi:10.1002/2015JC011178, 2016.

Van Der Veen, C. J.: Fracture mechanics approach to penetration of surface crevasses on glaciers, Cold Reg. Sci. Technol., 27(1), 31–47, doi:10.1016/S0165-232X(97)00022-0, 1998.

Vijay, S. and Braun, M.: Seasonal and interannual variability of Columbia Glacier, Alaska (2011-2016): Ice Velocity, Mass Flux, surface elevation and front position, Remote Sens., 9(6), 1–18, doi:10.3390/rs9060635, 2017.

Walter, J. I., Box, J. E., Tulaczyk, S., Brodsky, E. E., Howat, I. M., Ahn, Y. and Brown, A.: Oceanic mechanical forcing of a marine-terminating greenland glacier, Ann. Glaciol., 53(60), 181–192, doi:10.3189/2012AoG60A083, 2012.

Walters, R. A., Josberger, E. G. and Driedger, C. L.: Columbia Bay, Alaska: an "upside down" estuary, Estuar. Coast. Shelf Sci., 26(6), 607–617 [online] Available from: http://pubs.er.usgs.gov/publication/70013755, 1988.

Warren, C., Benn, D., Winchester, V. and Harrison, S.: Buoyancy-driven lacustrine calving, Glaciar Nef, Chilean Patagonia, J. Glaciol., 47(156), 135–146, doi:10.3189/172756501781832403, 2001.

Weertman, J.: Can a water-filled crevasse reach the bottom surface of a glacier?, Symp. Cambridge 1969 - Hydrol. Glaciers, 95, 139–145, doi:10.1017/CBO9781107415324.004, 1973.

Zeng, Q., Meisheng, C., Xuezhi, F., Fengxian, L., Xianzhang, C. and Wenkun, S.: Study on spectral reflection characteristics of snow, ice and water of northwest China., Sci. Sin. Ser. B, 27(145), 647–656, 1984.
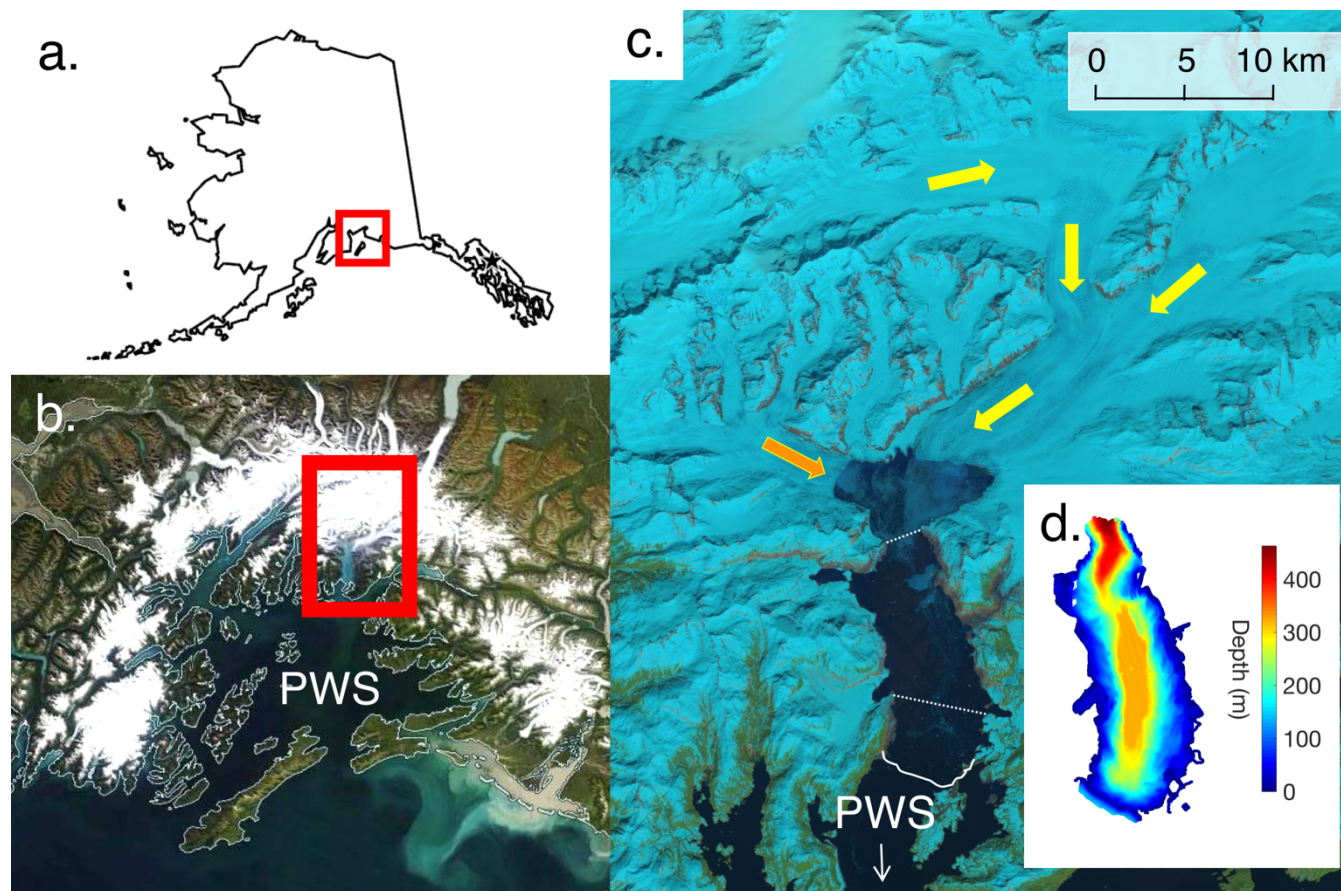
Figure 1: Columbia Glacier. **(a)** Outline of Alaska. **(b)** NASA MODIS image of PWS from World View satellite. **(c)** Landsat image of Columbia Glacier and Fjord in 2013. Yellow arrows indicate flow of the main branch of the glacier. Orange arrow indicates flow of west branch of the glacier. Heather Island is visible along Heather Moraine. Dotted lines delineate the boundaries between the Proximal Zone, the Mid-Fjord Zone, and the Distal Zone. White line indicates location of Heather Moraine. Inset **(d)** in panel **(c)** shows the bathymetry of Columbia Fjord measured by NOAA Ship RAINIER in 2005. The scale between **(c)** and **(d)** is 1:1.
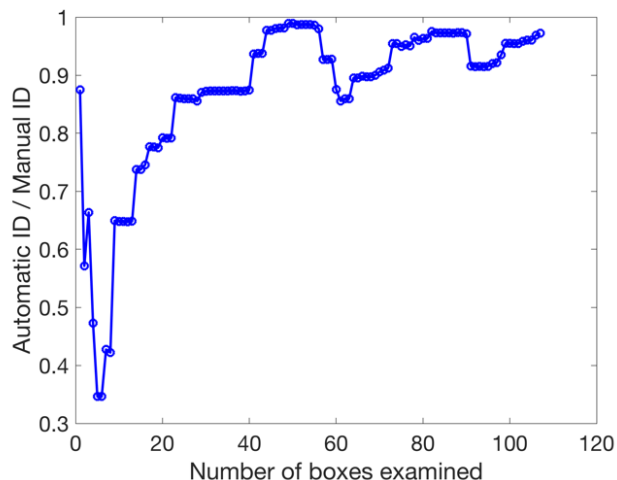
Figure 2: Ratio of automatic iceberg detection to manual iceberg detection as a function of the cumulative number of 250 x 250 pixel squares counted. The total number of boxes counted was 107.
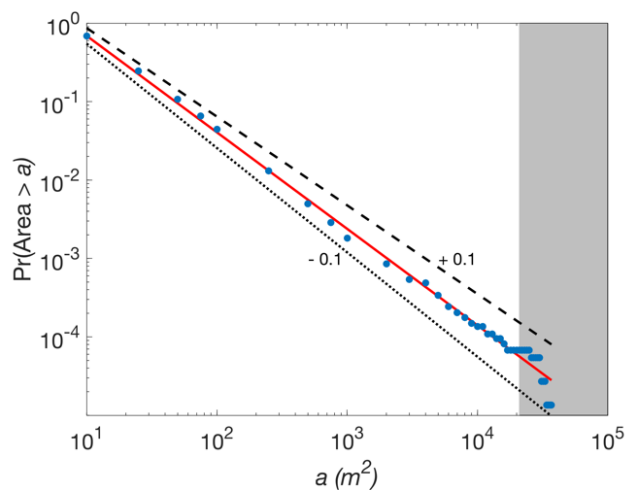
Figure 3: Power-law fit for the iceberg areas in the Proximal Zone on June 10b. The red line represents the best fit, and the black lines represent shifting the power exponent by ± 0.1 – the dotted line indicates a subtraction of 0.1, and the dashed line indicates an addition of 0.1. The icebergs that have been omitted to achieve a significant fit are plotted in the gray box.
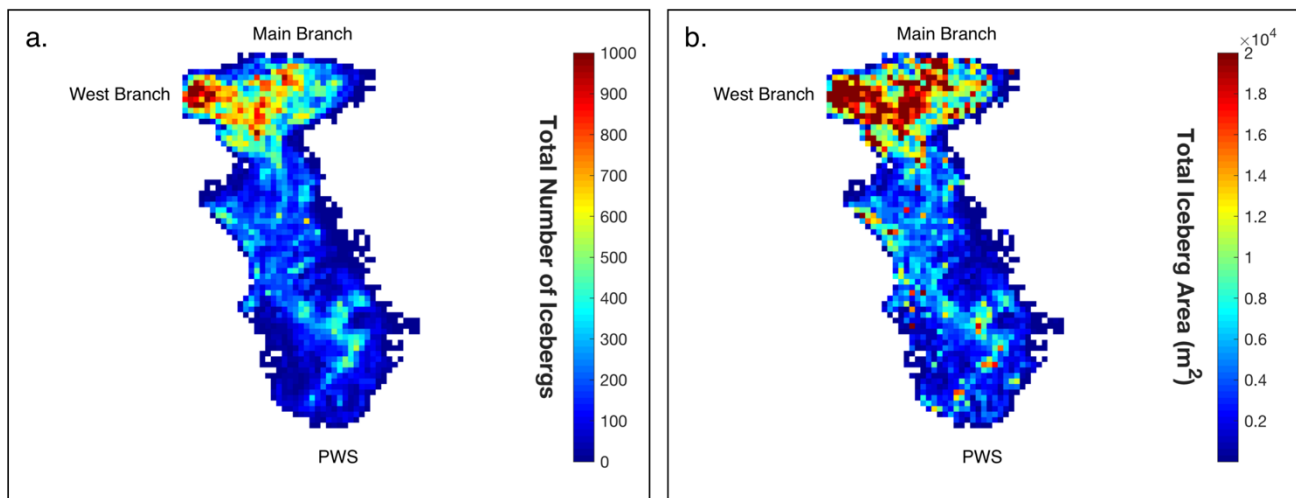
Figure 4: Cumulative iceberg population density and area map. Each grid cell represents a 500m x 500m square. The scenes from March 13, June 10a, July 12a, and November 19a were overlain to obtain the total number and area of icebergs inside each grid cell. **(a)** number of icebergs in each grid cell **(b)** area of icebergs inside each grid cell.
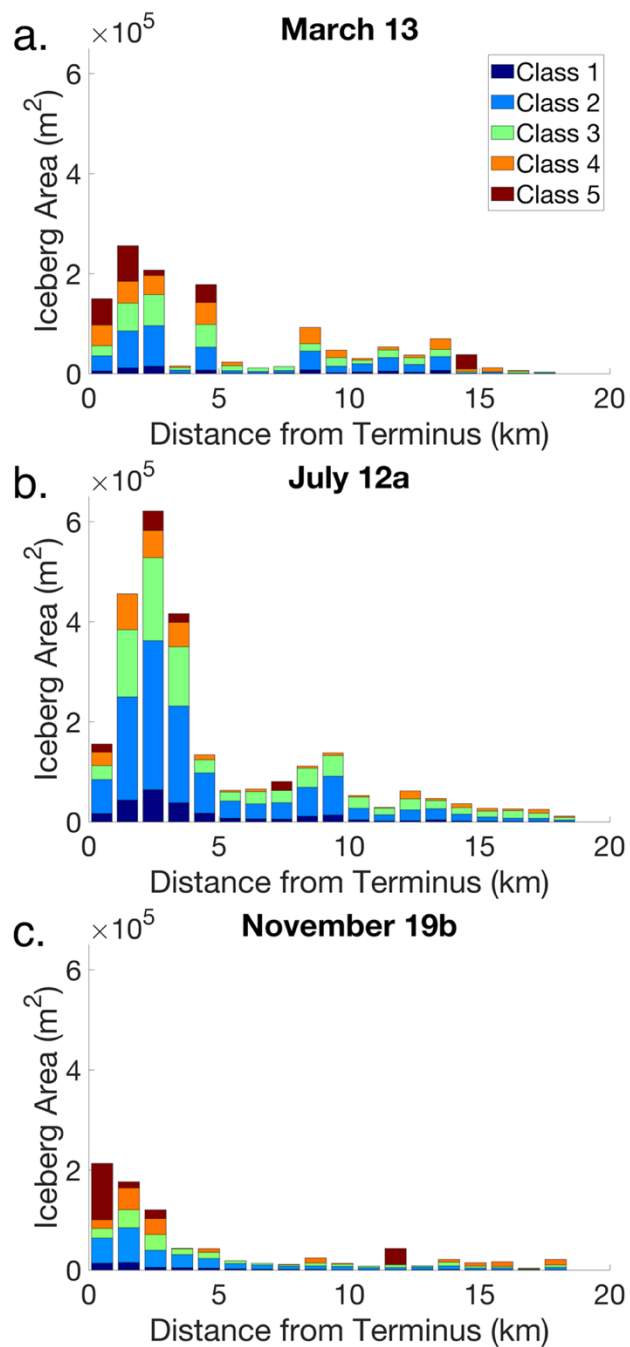
Figure 5: Total area of icebergs per 1 km bin along the fjord. The dates shown here are **(a)** March 13, **(b)** July 12, and **(c)** November 19. The peak of ice coverage inside the fjord is found 2-3 km from the terminus. The icebergs are divided into classes by waterline cross-sectional area, with the smallest icebergs residing in Class 1 and the largest in Class 5.
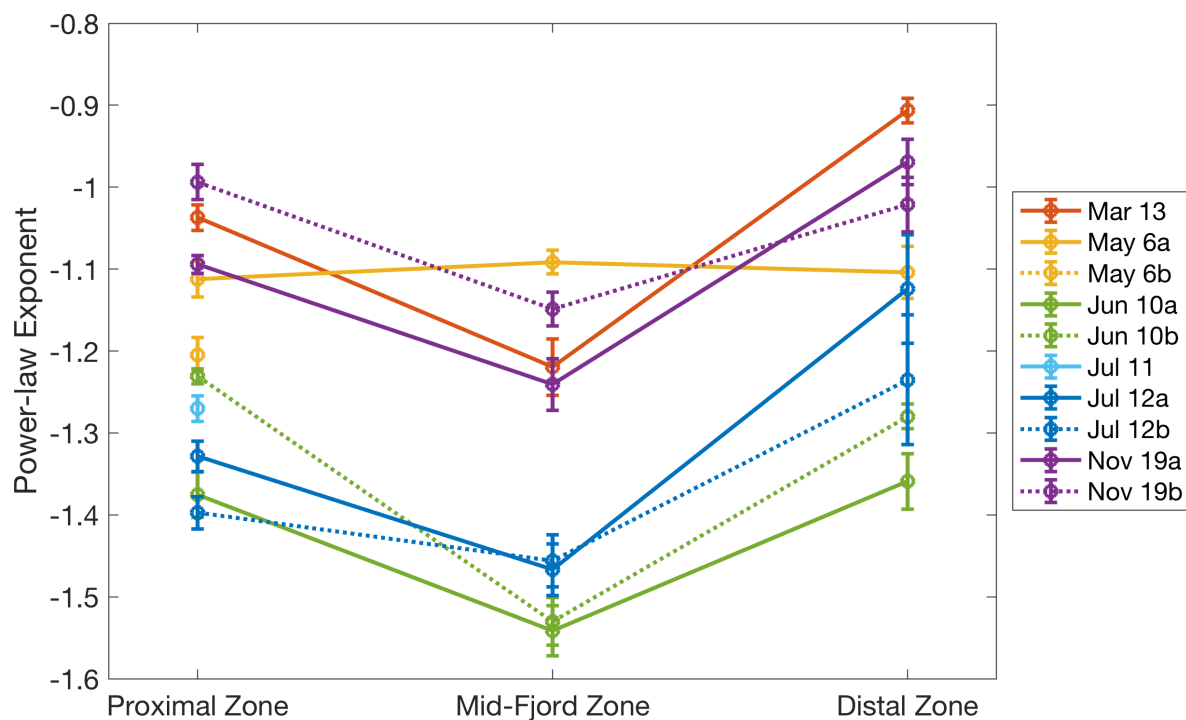
Figure 6: Power-law exponent calculated for each scene. Power-law exponents indicate both a spatial and seasonal discrepancy. The more positive exponent in the Proximal and Distal Zones indicate a higher proportion of large icebergs present near the terminus and Heather Moraine. Additionally, the more positive exponent for the spring and fall scenes indicates a higher proportion of large icebergs present in those respective seasons. The anomalous increase in the power exponent in the mid-fjord zone for May 6a is due to contamination from cloud cover.
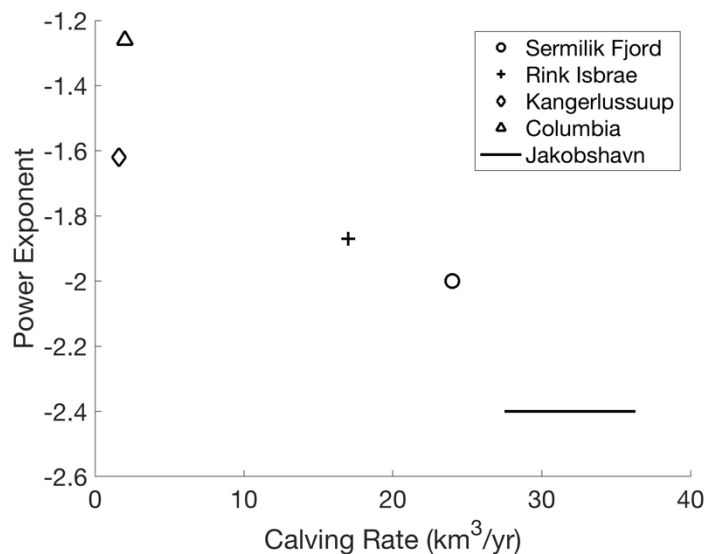
Figure 7: A comparison of published power exponents and glacier calving rates. (The power exponent for Columbia Fjord was calculated in this study.). An increase in the calving rate corresponds with an increase in the proportion of small icebergs present inside the fjord (more negative power exponent).
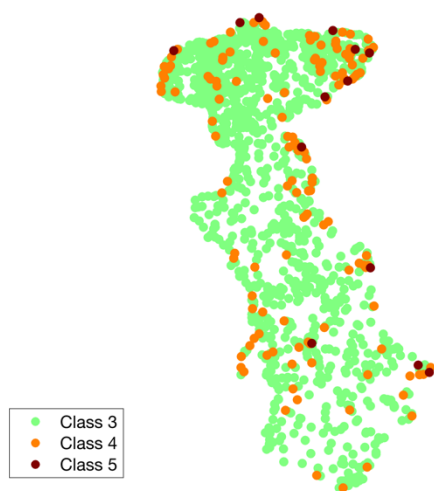
Figure 8: Location of large icebergs by centroid (May 06a).

Table 1: Survey of images used in this study. Image processing performed by Polar Geospatial Center prior to our obtaining the images. Satellites used were WorldView 1 and 2 (WV1, WV2). Projection is NAD83. *Time reported in AKDT

5 despite daylight savings ending on November 3.

Reference ID	Date, 2013	Alaska Daylight Time	Sensor	Coverage	Number of Images in Mosaic
March 13	March 13	13:14:44	WV1	Full	2
May 06a	May 06	13:32:05	WV2	Full	3
May 06b	May 06	13:33:02	WV2	Partial	2
June 10a	June 10	13:20:07	WV1	Full	3
June 10b	June 10	13:20:52	WV1	Full	3
July 11	July 11	12:51:12	WV1	Partial	3
July 12a	July 12	14:03:23	WV2	Full	3
July 12b	July 12	14:04:23	WV2	Full	3
November 19a	November 19	13:06:22*	WV1	Full	2
November 19b	November 19	13:07:18*	WV1	Full	2

Table 2: Correlation between different iceberg class sizes along the fjord for all scenes combined. The red shading corresponds to the size of the error estimates, with the darker shades of red representing larger error. Error is reported in lower half of table.

Size Classes	1	2	3	4	5
1		0.900	0.859	0.809	0.345
2	+ 0.025 - 0.033		0.980	0.840	0.394
3	+ 0.035 - 0.045	+ 0.005 - 0.007		0.863	0.391
4	+ 0.046 - 0.058	+ 0.039 - 0.050	+ 0.034 - 0.044		0.490
5	+ 0.125 - 0.138	+ 0.119 - 0.134	+ 0.119 - 0.134	+ 0.105 - 0.122	

Table 3: Volume of icebergs in Columbia Fjord for each scene, calculated using Eq. (2) and Eq. (3). The discrepancy in the total iceberg volumes presented for November 19a and November 19b are due to errors in iceberg identification. * Imagery of fjord is incomplete on these dates.

Date	Equation (3)			Equation (2)		
	Total Volume of Icebergs	Volume of Icebergs: Area > 1000m²	Percent Volume of Icebergs with Area > 1000m²	Total Volume of Icebergs	Volume of Icebergs: Area > 1000m²	Percent Volume of Icebergs with Area > 1000m²
Units	km³	km³		km³	km³	
March 13	0.077	0.065	84	0.060	0.042	70
May 06a	0.083	0.067	81	0.070	0.045	65
May 06b*	0.070	0.058	83	0.056	0.036	64
June 10a	0.10	0.055	53	0.12	0.042	35
June 10b	0.16	0.11	67	0.16	0.071	46
July 11*	0.12	0.089	72	0.11	0.054	50
July 12a	0.072	0.042	58	0.077	0.029	38
July 12b	0.074	0.041	56	0.079	0.029	36
November 19a	0.070	0.059	83	0.056	0.037	66
November 19b	0.057	0.050	88	0.042	0.031	74

Table 4: Increase in albedo of entire fjord due to presence of ice, calculated for each scene. Both icebergs and mélange are taken into account for the albedo calculations. Differences in albedo on November 19a and November 19b are due to errors in iceberg identification for November 19a.

Date	Relative Albedo Increase (%)
March 13	2.5 ± 0.95
May 06a	4.8 ± 1.8
May 06b	4.0 ± 1.5
June 10a	9.8 ± 3.7
June 10b	9.6 ± 3.6
July 11	6.2 ± 2.3
July 12a	7.7 ± 2.9
July 12b	7.4 ± 2.8
November 19a	3.7 ± 1.38
November 19b	1.2 ± 0.46